



UvA-DARE (Digital Academic Repository)

Hydrophobic modification of gamma-alumina membranes with organochlorosilanes

Sah, A.; Castricum, H.L.; Blik, A.; Blank, D.H.A.; ten Elshof, J.E.

DOI

[10.1016/j.memsci.2004.05.031](https://doi.org/10.1016/j.memsci.2004.05.031)

Publication date

2004

Document Version

Submitted manuscript

Published in

Journal of Membrane Science

[Link to publication](#)

Citation for published version (APA):

Sah, A., Castricum, H. L., Blik, A., Blank, D. H. A., & ten Elshof, J. E. (2004). Hydrophobic modification of gamma-alumina membranes with organochlorosilanes. *Journal of Membrane Science*, 243(1-2), 125-132. <https://doi.org/10.1016/j.memsci.2004.05.031>

General rights

It is not permitted to download or to forward/distribute the text or part of it without the consent of the author(s) and/or copyright holder(s), other than for strictly personal, individual use, unless the work is under an open content license (like Creative Commons).

Disclaimer/Complaints regulations

If you believe that digital publication of certain material infringes any of your rights or (privacy) interests, please let the Library know, stating your reasons. In case of a legitimate complaint, the Library will make the material inaccessible and/or remove it from the website. Please Ask the Library: <https://uba.uva.nl/en/contact>, or a letter to: Library of the University of Amsterdam, Secretariat, P.O. Box 19185, 1000 GD Amsterdam, The Netherlands. You will be contacted as soon as possible.

UvA-DARE is a service provided by the library of the University of Amsterdam (<https://dare.uva.nl>)

Instrumentation for Δ photoproduction experiments on nuclei with high energy resolution

G. van der Steenhoven*, H.L. Castricum, L. Lapikás,
G.J.L. Nooren, M. Schroevers, J.J.M. Steijger and M.A. van Uden

*Nationaal Instituut voor Kernfysica en Hoge-Energiefysica (NIKHEF),
P.O. Box 41882, 1009 DB, Amsterdam, The Netherlands*

() Corresponding author; tel.: +31-20-592 2145, fax: +31-20-592 5155, e-mail:
gerard@nikhef.nl*

E. Cisbani, S. Frullani, F. Garibaldi, M. Iodice, G.M. Urciuoli

Istituto Nazionale di Fisica Nucleare (INFN), Sanitá, Roma, Italy

D. W. Higinbotham

*Department of Physics, University of Virginia, Charlottesville,
Virginia, United States of America*

A technique has been developed to perform photo-induced experiments in the region of the $\Delta(1232)$ resonance with a sufficiently good energy resolution to separate excited states of the final nucleus. The technique utilizes developments in accelerator technology (high-duty factor electron beams), target technology (multi-layer waterfall targets), and detector technology (diffusely reflective aerogel Čerenkov systems). Taken together, these developments have enabled studies of the reaction $^{16}\text{O}(\gamma, \pi^- p)$ with an energy resolution of less than 1 MeV. This represents an order of magnitude improvement in energy resolution over previous experiments of this kind.

1 Introduction

The interest in experiments in which a $\Delta(1232)$ -resonance is produced inside the nucleus, stems from the possibility to use such reactions for the study of the poorly known nucleon- Δ interaction [1]. In order to reconstruct the momentum of the propagating Δ -resonance, it is essential to detect its two decay products

(a pion and a nucleon) in coincidence and measure their momenta precisely. In the past such experiments have been carried out using secondary pion beams as a probe. However, the photon is the probe of choice for such studies as it reduces complications related to initial-state interactions, and ensures that the entire nuclear volume contributes to the reaction yield.

Thusfar, several $(\gamma, \pi^- p)$ experiments have been reported in the literature [2–6]. These measurements suffered from a poor energy resolution (≈ 10 MeV) and—in most cases—poor statistics. It is difficult to obtain high statistics results in a $(\gamma, \pi^- p)$ experiment, as the cross section for the reaction is low. For this reason it is desirable to perform such experiments using the end-point of a Bremsstrahlung beam since it produces an instantaneous photon flux that is several orders of magnitude larger than is available either from tagged photon or laser-backscattering techniques. The use of a Bremsstrahlung beam makes it particularly important to have good energy resolution, as the cross sections are extracted from such data by means of an end-point-fit taking the known shape of the Bremsstrahlung spectrum as input [7]. Any uncertainty in the starting point of the Bremsstrahlung shape introduces large systematic uncertainties in such fits, as is particularly evident in the analysis of ref. [3]. Hence, it is crucial to have good energy resolution, a correspondingly good energy calibration, and good statistics. Although some of the aforementioned $(\gamma, \pi^- p)$ experiments had reasonable statistics, none of them had a good energy resolution (for an overview see ref. [8]).

An additional motivation for carrying out $(\gamma, \pi^- p)$ experiments with good energy resolution is that this reaction can also be used for the determination of spectroscopic factors and radii of neutron orbitals inside nuclei [8,9]. The good energy resolution is necessary to identify the final state; and thus, to determine the quantum numbers of the orbital involved.

In order to pursue these goals we improved the technique for carrying out $(\gamma, \pi^- p)$ experiments in such a way that both high statistics and high energy resolution can be obtained. An electron beam is used to produce a beam of real and virtual photons inside a target, which is also used as reaction target. It was not needed to use a separate radiator target with a deflection system in front of the reaction target to bent the electron beam away, as the time-structure of the beam and the chosen detector system allowed to record the electron and photon-induced events simultaneously without causing any dead-time problems. The required instrumentation for this technique is briefly described below.

- A high-duty factor electron beam is used to produce an almost continuous (virtual) Bremsstrahlung beam. The high-duty factor is essential in order to reduce the background of accidentally coincident pion–proton pairs. In our case use was made of the extracted electron beam from the Amsterdam

- Pulse Stretcher [11].
- A triple-layer waterfall target makes it possible to increase the overall luminosity while maintaining the resolution associated with measurements employing a thin foil.
- High-resolution magnetic spectrometers are used to detect both the pions and protons, and determine their momenta. The use of spectrometers goes at the expense of solid angle, and therefore makes it mandatory to use high-intensity photon beams and large target thicknesses at the same time. In the present case the high-resolution spectrometer pair of the EMIN hall at NIKHEF was used, which is described in [12]. The QDD spectrometer is used for proton detection and the QDQ spectrometer for pion detection.
- A Čerenkov detector is needed for the identification of negative pions amidst a huge background of electrons. The Čerenkov detector, along with an additional scintillator, were added to the detector package of the QDQ spectrometer.
- A high speed data-acquisition system allows the full read-out of all coincident events. This makes it possible to distinguish between $(e,e'p)$ and (γ,π^-p) events in the off-line analysis. Hence, it is not necessary to implement and use a hardware pion-trigger from the Čerenkov signals as was common in the past [13].

As several components of our set-up have been described elsewhere, the present discussion is limited to a description of the waterfall target (section 2), the Čerenkov counter and added scintillator in the QDQ focal plane (section 3), some aspects of the data-acquisition system (section 4), and the overall performance of the set-up (section 5). The paper ends with a brief summary and outlook (section 6).

2 The waterfall target

The basic technique of (γ,π^-p) experiments with high energy resolution could have been demonstrated on any target with a modest level spacing. However, there are clear advantages to using ^{16}O as the target nucleus, because advanced Distorted-Wave Impulse Approximation (DWIA) Δ -propagation calculations for the reaction $^{16}\text{O}(\gamma,\pi^-p)$ [9,10] have now become available. These will allow for a careful interpretation of the data. Moreover, most of the previous work studying Δ -propagation in nuclei was also based on ^{16}O (see references [3,16], for instance).

Compared to other options it is advantageous to use water as an oxygen target for the present application. Pure oxygen is difficult to handle, as it is highly reactive and thus requires safety measures. The use of other oxygen compounds results in additional measurements that are needed to subtract the non-oxygen

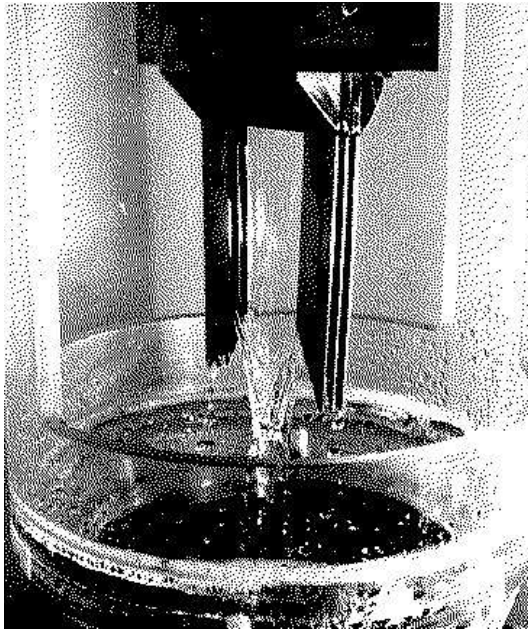


Fig. 1. *Photograph of the three-film waterfall target developed for the present experiment. The target is shown in a separate test set-up. It is not visible during normal operation in the electron scattering environment.*

background. On the other hand the hydrogen content of a water target does not cause any complications, as the reaction $(\gamma, \pi^- p)$ cannot occur on a free proton.

The technique of using continuously flowing water as an electron scattering target was first developed by Voegler and Friedrich [17], and later refined by Garibaldi et al. [18]. Such a target consists of a thin film of water falling down while guided by two metal rods on the side. For the present experiment the design was further improved by creating three thin water films in parallel and with a mutual distance of 3 mm. This is illustrated in figure 1.

The waterfall target is placed in a hydrogen atmosphere, which is separated from the beamline vacuum by means of a $25 \mu\text{m}$ foil of stainless steel. The hydrogen was kept at a pressure of 1.1 bar. The target thickness was determined from elastic electron scattering measurements, yielding a total thickness of about 205 mg/cm^2 which correspond to a typical thickness of 68 mg/cm^2 for each water film. The statistical error in these values is rather small (1%), while the systematic uncertainty is somewhat larger (3%) due to the size of the error in the existing elastic electron scattering data off oxygen [19]. During a two-week period of data taking the target thickness was measured to be stable to within 3.4 % as observed from the single rates in the spectrometers. This spread includes variations due to changing beam conditions.

In order to exploit the availability of three separate water films, it must be possible to track the scattered particles back to their target coordinates. The

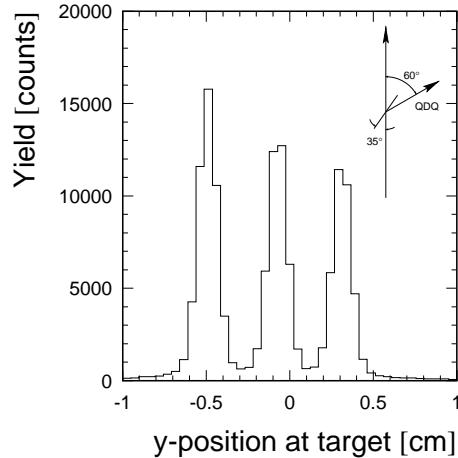


Fig. 2. *Reconstructed spectrum of the scattering vertex, showing the separation of events originating from different films in the water target. The x-axis represents the coordinate perpendicular to the optical axis of the QDQ spectrometer. The inset shows the position of both the spectrometer and the water target with respect to the incoming electron beam.*

precise knowledge of the spectrometer matrix elements [20] enables such a reconstruction. This is illustrated in figure 2, where the spectrum of scattered electrons is shown as a function of the coordinate perpendicular to the optical axis of the QDQ spectrometer. A clear separation is observed of events coming from different water films.

Since the film in which an event occurs is known, the energy loss of both the pion and the proton can be evaluated with greater precision, resulting in a smaller contribution to the overall energy resolution from the target. This multi-layer technique was first pioneered in an electron scattering experiment by Bobeldijk et al. [21].

3 New detectors for the QDQ spectrometer

In the presently proposed technique of performing $(\gamma, \pi^- p)$ measurements, the target is exposed to a mixed beam of electrons and photons. Therefore, the detector system located in the focal plane of the pion spectrometer (QDQ) must be able to discriminate between negative pions and electrons. Previously, the QDQ detection system has been extensively used for high-resolution $(e, e'p)$ experiments [12]; but now, with the addition of the aerogel Čerenkov detector and the Top scintillator the system can also be used for electron-pion separation. Apart from these additions, the system comprises a set of 4 Multi-Wire Drift Chambers (MWDC's) for tracking, and two scintillator arrays for trig-

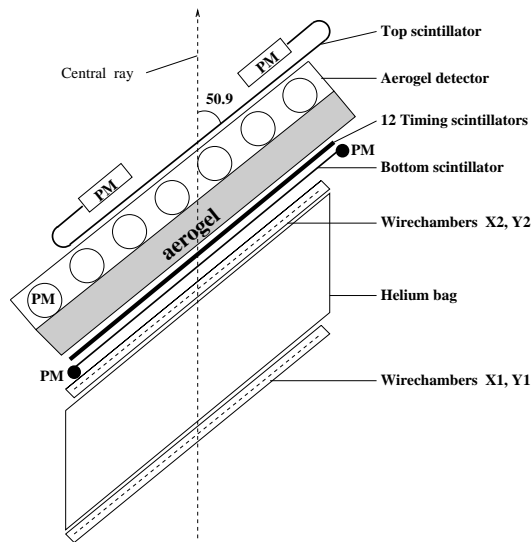


Fig. 3. *Detector package in the focal plane of the QDQ spectrometer in the EMIN hall at NIKHEF. The various components are indicated.*

gering purposes. In between the two sets of MWDC's a bag filled with helium gas is placed, in order to decrease the effect of multiple scattering on the accuracy of the angular track reconstruction of low-energy particles. The complete system as it is used for $(\gamma, \pi^- p)$ measurements is shown in figure 3. In the following two subsections the construction and commissioning of the two new detectors in the QDQ spectrometer is discussed.

3.1 The Čerenkov detector

The Čerenkov detector consists of a rectangular light-tight aluminium box of inner dimensions $1333 \times 140 \times 203 \text{ mm}^3$, which is partly filled by a (10 ± 0.2) cm thick layer of aerogel with a refractive index of $n = 1.05$. The aerogel layer consists of 28 blocks of $19 \times 14 \text{ cm}^2$ with different thicknesses ranging from 2 to 3 cm. Since the detector is placed in the QDQ spectrometer at an angle of 50.9° with respect to the central particle path, the detector has an effective aerogel thickness of 12.9 cm. Photons are produced in the aerogel when the speed of a charged particle passing through the detector is greater than the speed of light in the aerogel.

The light box region, i.e. the region outside the aerogel where the photons are reflected and detected, is viewed by seven 5" Philips XP-2041Q photomultiplier tubes. The diffusely reflective walls of the aluminium box are covered by Millipore¹ paper type GSWP00010 except for the wall to which the photomultiplier tubes are attached. This wall is painted with Eastman Reflective

¹ Millipore Corporation, 80 Ashby Road, Bedford, MA 01730

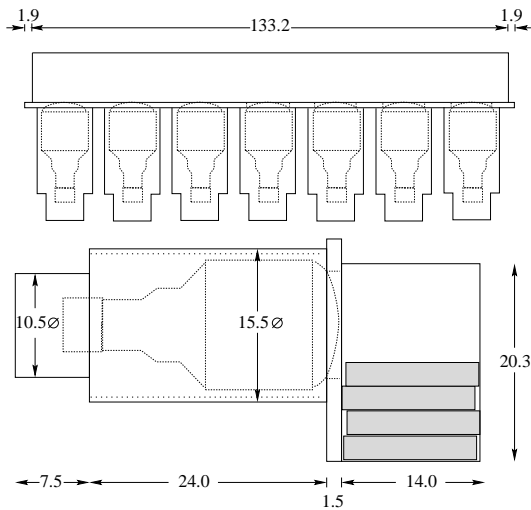


Fig. 4. Schematic diagram of the Čerenkov detector of the QDQ spectrometer in the EMIN hall at NIKHEF. Both the top view (above) and the side view (below) of the detector are shown. The measures are in cm.

Coating, a highly reflective paint which is unfortunately no longer being produced. Both the paint and the Millipore paper have been shown to have diffuse reflectivities of 96% in the region of interest [22], while the reflectivity of the aerogel surface is only 80% [24]. A schematic of the detector’s design is shown in fig. 4.

3.1.1 Refurbishment

The Čerenkov detector which we are using was originally built in 1983. At this time an average signal of 17 photoelectrons per $\beta = 1$ particle passing through the detector was observed [13]. The detector was used for three years before being removed and placed in storage.

When the detector was removed from storage in 1993, a visual inspection of the detector showed that much of the normally translucent, colorless aerogel had turned yellow. This is probably due to contaminations being trapped in the material, rather than radiation damage as the aerogel material itself is known to be radiation hard [25]. Since the diffusely reflective walls may suffer from aging [24], it was decided that the detector needed to be refurbished.

Refurbishing of the Čerenkov detector involved changing the aerogel and the diffusely reflective walls. No changes were made to the photomultiplier tubes or their bases. Though the tubes and bases may not be as efficient as they originally were, they still work quite well and it was not considered necessary to either replace or refurbish them.

Aerogel pieces, which showed high levels of visible contamination, were dis-

carded and replaced by new blocks from Airglass²; while other pieces, which showed little visible contamination, were put aside to be baked, a known method of removing a large percentage of contaminants from aerogel. The baking was done by slowly heating the aerogel over the course of eight hours to 500° Celsius. The blocks were then kept at this temperature for two hours and then the oven was slowly turned off over another eight hours. The oven was open to dry air during the entire procedure so that the contaminating molecules could be flushed away. Care must be taken when reheating aerogel blocks as heating can cause structural changes in the aerogel which will increase its refractive index [23].

The final 28 blocks of aerogel which were reinstalled in the Čerenkov detector consisted of 17 baked old blocks and 11 new blocks. The blocks were placed in the detector in four layers and held in place by two thin steel wires. The diffusely reflective walls of the detector were refitted with two new layers of Millipore filter paper held in place by double sided tape.

No steps were taken to decrease the previous rate of contamination. Such steps could have included the use of non-outgasing glues, and flushing the detector with inert gas. However, the latter process has only been used with minimal success in the past [24].

3.1.2 Simulations

Simulations were done to see how well the original photoelectron value and the refurbished Čerenkov detector’s photoelectron value compared to the values of other Čerenkov detectors. Two different methods, a phenomenological equation and a computer simulation, were used to make these comparisons. Both methods are described in detail in ref. [26].

The phenomenological equation is based on the previous results of existing aerogel detectors, and can be used to obtain an easy estimate of the relative performance of a new detector using its global features as input. The equation is written

$$N_e = HL(1 - 1/\beta^2 n^2) \frac{\epsilon z^2}{1 - \eta(1 - \epsilon)}, \quad (1)$$

where N_e is the number of photoelectrons, L is the path length of a charged particle through the aerogel, n is the refractive index of the aerogel, β is the velocity of the charged particle divided by the speed of light, ϵ is the fraction of the light box area covered by photomultiplier tubes, η is the average reflectivity of the light box area, and z the charge of the particle passing the aerogel. For

² Airglass Inc., Lund, Sweden

the present detector the quantity ϵ has a value of 0.096. The quantity η has been evaluated using the prescribed 96% reflectivity for the diffusely reflective walls, and the effective 80% reflectivity for the aerogel, yielding $\eta = 0.92$. The figure of merit H contains all other factors on which the number of produced photoelectrons depends, notably the scattering and absorption length of the aerogel. Therefore, H will depend on L as well. For a value of L around 12.9 cm the values of the H parameter are found to be between 19.3 and 28.5, corresponding to an expected signal of between 12 and 18 photoelectrons [26].

The computer simulation uses the same variables as the phenomenological equation plus information about geometry and tube placement. All other parameters have been set to nominal values within the computer code and are not changed from one simulation to the next. The simulation calculates the number of photoelectrons directly using the equation

$$N = \int_{\lambda_1}^{\lambda_2} 2\pi\alpha L \left(1 - \frac{1}{\beta^2 n^2}\right) \frac{z^2}{\lambda^2} d\lambda \quad (2)$$

where N is the number of photons, λ is the wavelength of the photons, and α is the fine structure constant. The diffuse reflections of the photons through the light box region are simulated using a monte-carlo code. The program focusses on the tracking of the photons in the light box region, while the effects of the aerogel itself are estimated from its bulk properties.

By taking into account the detector geometry and tube placement, the computer simulation can generate not only information about the number of expected photoelectrons; but also, information about detector uniformity, timing, and photomultiplier multiplicity—the number of different tubes that fire per event. The computer simulation predicts an average signal of 15 photoelectrons for the present aerogel Čerenkov counter, a multiplicity of 4 photomultipliers, and excellent uniformity. These predictions will be compared to the test results in section 5.1.

3.2 *The Top scintillator*

The Top scintillator consists of a long slab of dimensions $1280 \times 140 \times 4 \text{ mm}^3$, which has a slightly smaller acceptance as the aerogel Čerenkov detector due to the limited amount of room available for the PMT at the top end of the scintillator in the shielding hut of the QDQ spectrometer. The scintillator, which is of the type BC400, is loosely wrapped in aluminium foil and a layer of light-tight plastic. It is read out on each end by a 2" EMI 9954b photomultiplier tube. These are connected to the scintillator by means of twisted light guides.

The light guides are wrapped in highly reflective aluminized mylar to reduce the light loss in the bend and are covered with black plastic tape. Scintillator, light guides, PMT's, and bases are kept together by an aluminium frame which in turn is fixed to the Čerenkov detector. The detector's position in the QDQ focal plane is shown in figure 3.

During the measurements the new Top scintillator operated well yielding clear signals for both pions and electrons, the size of which depended on the applied high voltage on the PMT's.

The scintillator can be used to set-up a hardware pion trigger [13], but this is not necessary in the presently described technique of $(\gamma, \pi^- p)$ measurements at high-duty factor beams. The scintillator has been used, though, to measure the efficiency of the Čerenkov detector for electron detection. At two different values of the momentum setting of the QDQ spectrometer electron efficiencies of 99.9 % were found.

4 Data-acquisition system

In this section a brief description is given of the data-acquisition system used in the present set-up. It is based on the standard NIKHEF data-acquisition system which treats each detector in the experiment as an independent unit, which generates a trigger (Arm-TRigger, ATR) the phase of which is set by the passage of the particle through the physical detector, stores the measured information locally, and sends that information on receipt of a read-out or event trigger to the event builder. The coincidence detector takes the ATR's from all detectors and determines the timing relations between these signals. When one (or more) of the maximum 31 predefined conditions is met an event trigger (ETR) is generated and sent to the detectors involved in the event.

This system allows easy expansion of any detector, as was needed in this case when the aerogel and top scintillator were added to the existing QDQ-spectrometer. Figure 5 shows the separate read-out of these components, sharing the same ATR and ETR signals, and an extra node which tacks the extra information on the end of the QDQ event descriptor. The result looks the same as any other detector arm, and can be used in the data-acquisition system without any changes.

The data-acquisition system has a maximum throughput of about 4500 events per second. In the present application it was operated well below this limit, resulting in dead-time corrections below the level of 0.1 %.

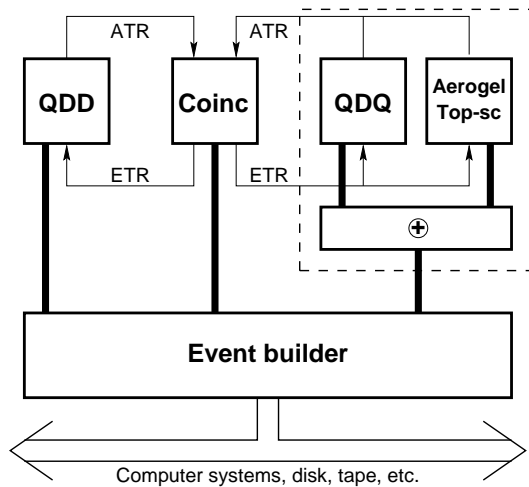


Fig. 5. Schematic representation of the data-acquisition system. To the right is the expanded read-out of the QDQ-spectrometer, which includes the new aerogel and top scintillator. The dashed box shows that the new configuration is equivalent to the original QDQ read-out.

5 Results

In this section we present the results obtained with the detector systems when the waterfall target was exposed to a high-duty factor electron beam of $7 \mu\text{A}$ extracted from the stretcher ring AmPS. Beam energies of 369 and 516 MeV were used, while the momentum setting of the QDQ spectrometer varied between 160 and 330 MeV/c. The successful operation of the triple-film waterfall target was already mentioned in section 2, and will not be further addressed. The performance of the Čerenkov detector is the subject of section 5.1, while the performance of the entire system is discussed in section 5.2.

5.1 Performance of the Čerenkov detector

Figure 6 shows the sum of the (gain and pedestal corrected) ADC spectra of the seven PMT's. The large number of events centered around channel 0 corresponds to pions that do not generate Čerenkov light. The peak centered around channel 425 can be used to estimate the number of photo-electrons generated by the passage of an electron with momentum 213 MeV/c ($\beta = 1$). Following ref. [13] the width of the peak is assumed to be Gaussian, and corresponds to the observation of about 13 photo-electrons.

The ability of the Čerenkov detector to discriminate between negative pions and electrons can be expressed in terms of the electron rejection ratio, which is defined as the total number of electrons over the number of electrons below the cut (between π^- and e events) Dunn [13] found a value of about 10^5 for

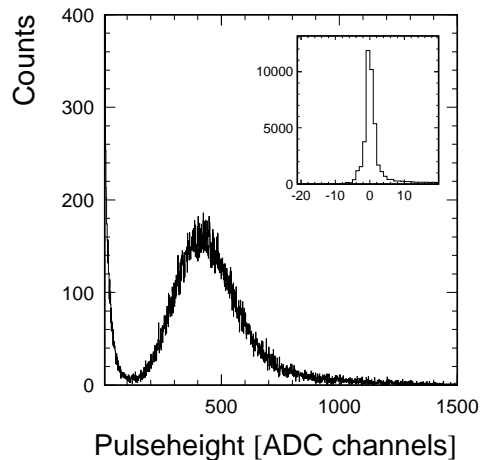


Fig. 6. *Response of the aerogel Čerenkov detector obtained at an incident electron energy of 525 MeV and the central QDQ momentum set to 213 MeV/c. The data represent the sum of the ADC-signals of each of the 7 PMT's. Corrections have been applied for pedestal and gain differences. Both the pion peak around channel 0 (inset), and the electron peak at channel 425 are shown.*

this ratio, while in the present case the ratio is down to 10^3 (with a cut at 3 photo-electrons).

For the present application it makes more sense to describe the quality of the detector in terms of the probability that an electron is identified as a pion, i.e the electron contamination. For the refurbished detector the contamination of the pion signal by electrons was found to range from 0.2 % to 1.0 % depending on momentum and angle setting of the spectrometer. Hence, the system is well suited for the clean identification of pions in an electron scattering environment.

In figure 7 the response of the summed analogue signals of the seven PMT's of the Čerenkov detector (for $\beta = 1$ particles) is compared to the results of the computer simulation. In the figure the ADC channel numbers have been converted to number of photo-electrons. The experimental average signal of 13 photoelectrons corresponds well with the computer-predicted average number of 15 photo-electrons. When compared to the 17 photoelectrons found with the original detector [13], it would seem that the quality of the detector has gone down; though both results lie within the nominal range of between 12 to 18 photo-electrons as obtained in section 3.1.2. Since this nominal range is determined from the performance of existing aerogel Čerenkov detectors, it is concluded that the refurbished detector yields a signal that is comparable to that of other diffusely reflective aerogel Čerenkov detectors.

The multiplicity of the Čerenkov detector — the number of PMT's which fire

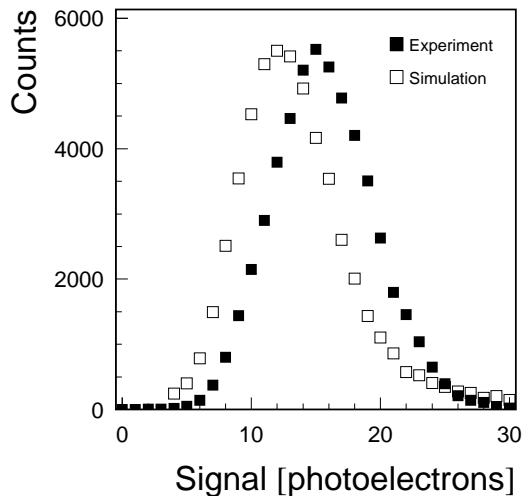


Fig. 7. Response of the Čerenkov detector of the QDQ spectrometer in the EMIN hall at NIKHEF. Both the results of a simulation (dark squares) and those of the actual measurements (open squares) are shown. For the data the ADC channel number has been converted to the equivalent number of photo-electrons. The curves are shown with the same number of events.

per $\beta=1$ event — is compared to that of the simulations in figure 8. In both the experimental and the simulated data an average of 4 PMT’s fire when a charged $\beta = 1$ particle passes through the detector. This shows that even in a relatively large detector the diffusely reflected light scatters over a large region and is not confined to the small region of the light cone, in which the Čerenkov light is radiated.

5.2 The reaction $^{16}\text{O}(\gamma, \pi^- p)$

The quality of the entire set-up for high-resolution $(\gamma, \pi^- p)$ measurements has been investigated by exposing the triple-film water target to a $7 \mu\text{A}$ high-duty factor electron beam from AmPS. The magnetic field and angle of the spectrometers were chosen such that the first 20 MeV of the $^{16}\text{O}(\gamma, \pi^- p)$ end-point spectrum was included in the acceptance. Events with a coincident signal in both spectrometers were recorded. It has to be realized that a spectrometer setting for $(\gamma, \pi^- p)$ measurements will always result in the simultaneous observations of $(e, e'p)$ events, as the trigger in the QDQ spectrometer does not include any requirement on the particle identification.

In the off-line analysis the measured flight-time difference between the two coincident particles was plotted versus the aerogel response. The results are displayed in figure 9. A clean separation of electrons and negative pions is observed. These results demonstrate the possibility of cleanly identifying $(\gamma, \pi^- p)$

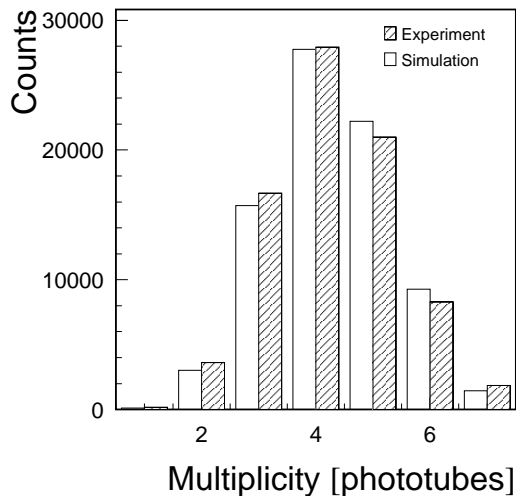


Fig. 8. Multiplicity of the Čerenkov detector of the QDQ spectrometer in the EMIN hall at NIKHEF. Both the results of a simulation (dark histogram) and those of the actual measurements (light histogram) are shown. The high average number of tubes firing per event demonstrates how the diffusely reflective walls scatter the Čerenkov radiation over the entire light box region.

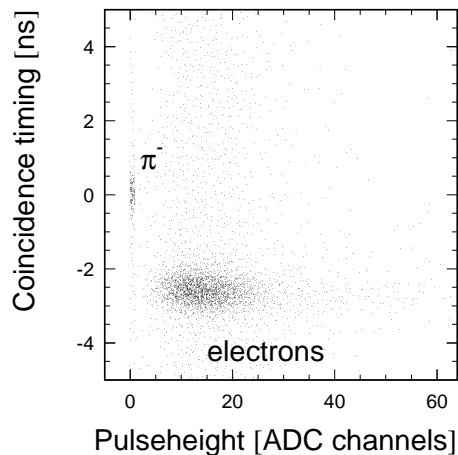


Fig. 9. Correlation between the timing difference between the two spectrometers signals (coincidence timing) and the ADC signal of the Čerenkov detector of the QDQ spectrometer in the EMIN hall at NIKHEF. The regions associated with pion and electron events are indicated.

events amidst a huge background of $(e,e'p)$ events.

In a next step the excitation-energy spectrum of the residual ^{15}O nucleus has been determined for the coincident proton-pion events. The physics result of this $^{16}\text{O}(\gamma,\pi^-p)$ experiment will be described elsewhere [27]. A typical spectrum is reproduced in figure 10. The spectrum shows the superposition

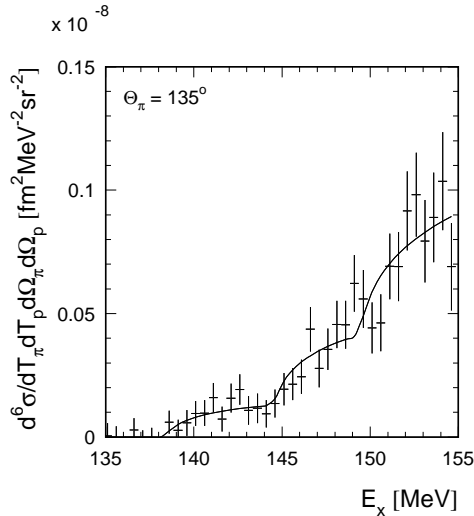


Fig. 10. *Bremsstrahlung endpoint spectrum for the reaction $^{16}\text{O}(\gamma, \pi^- p)$ as obtained with the QDD and QDQ spectrometers in the EMIN hall at NIKHEF. The energy scale corresponds to the missing energy of the reaction corrected for the Q -value of the reaction. As a result the ground state transition will start at the pion mass. The curve corresponds to an end-point fit of the data.*

of three end-point curves that are characteristic for experiments induced by Bremsstrahlung photon beams. Most importantly, though, is the remarkably clear separation between the ground-state transition corresponding to the removal of a $1p_{1/2}$ neutron, and the transition at 6 MeV excitation energy corresponding to the removal of a $1p_{3/2}$ neutron. These transitions have never before been separated in a $(\gamma, \pi^- p)$ experiment.

Also shown in figure 10 is the result of an end-point fit, which is needed for the extraction of cross sections. The statistics close to the end-point did not allow a precise determination of the energy-resolution using an energy-smearing Gaussian distribution. In fact, a good end-point fit has been obtained without any resolution smearing. It is concluded that the energy-resolution must be of the order of a few bin widths (0.5 MeV), or less.

6 Conclusions

A new technique for carrying out Δ -photoproduction experiments has been developed. It is based on using high-duty factor electron beams producing a beam of virtual and real photons in the scattering target. The high photon flux of such a Bremsstrahlung beam enables the use of high resolution magnetic spectrometers for the detection of the decay products of the Δ resonance. As the scattering target is exposed to both the (virtual) photon flux and the incident electron beam, the detectors in the focal plane of one of the

spectrometers need to be able to discriminate between negative pions and electrons. To this end an existing 14 year old aerogel Čerenkov detector was successfully refurbished. In this way a well-operating aerogel detector was obtained against minimal costs. The performance of the Čerenkov detector was in accordance with the simulations.

In order to investigate the prospects of this technique a dedicated $(\gamma, \pi^- p)$ experiment has been carried out on a newly developed waterfall target. The combined use of high-duty factor electron beams, high-energy resolution magnetic spectrometers equipped with a Čerenkov detector, and a multi-film water target enabled us to obtain $^{16}\text{O}(\gamma, \pi^- p)$ spectra with an energy resolution of less than 1 MeV. This represents an improvement compared to previous work [3] by one order of magnitude.

Following the successful commissioning of this technique for $(\gamma, \pi^- p)$ experiments, it has also been tried to replace one of the spectrometers by a large-acceptance scintillator array. In this way it is possible to increase the proton solid angle from about 6 msr to 200 msr at the expense of resolution (back to 5 MeV). Also in this case, we were able to extract $(\gamma, \pi^- p)$ data, albeit of lower resolution [28].

The use of these techniques will make it possible to explore the Δ -N interaction in nuclei, now that intense high-duty factor electron beams have come available at TJNAF and Mainz. As both laboratories are equipped with pairs of high-resolution spectrometers, the $(\gamma, \pi^- p)$ reaction can be investigated in a systematic fashion and — as the available photon energies become higher — extended to the study of various Baryon resonances.

This work is part of the research program of the FOM-institute for subatomic physics, NIKHEF, which is financially supported by the Netherlands' Organisation for Scientific Research (NWO). One of the authors (DWH) was supported by DOE grant DE-FG05-87ER40364. The work of S. Colilli, R. Crateri, M. Gricia, M. Lucentini and F. Santavenere on the waterfall target is acknowledged.

References

- [1] J.M. Laget, Proceedings of the NATO Study Conference on New Vistas in Electro-Nuclear Physics, eds. E.L. Tomusiak, H.S. Caplan and E.T. Dressler, NATO ASI Series, **B142** (1986) 361.
- [2] I.V. Glavanakov and V.N. Stibunov, Sov. J. Nucl. Phys. **29** (1979) 746; and Sov. J. Nucl. Phys. **30** (1979) 465
- [3] L.D. Pham *et al.*, Phys. Rev. **C46** (1992) 621

- [4] L.B. Weinstein *et al.*, Phys. Rev. **C47** (1993) 225
- [5] J.D. MacKenzie *et al.*, Phys. Rev. **C54** (1996) 6
- [6] K. Hicks *et al.*, Phys. Rev. **C55** (1997) R12
- [7] L. Tiator and L.E. Wright, Nucl. Phys. **A379** (1982) 407
- [8] G. van der Steenhoven, Proc. of the 7th Amsterdam mini-conference on *Electromagnetic production of mesons on nucleons and nuclei*, eds. H.P. Blok, J.H. Koch and H. de Vries, Amsterdam (1991) p. 92
- [9] X. Li, L.E. Wright, and C. Bennhold, Phys. Rev. **C48** (1993) 816
- [10] T. Sato and T. Takaki, Nucl. Phys. **A562** (1993) 673
- [11] P.K.A. de Witt Huberts, Nucl. Phys. **A553** (1993) 845c
- [12] C. de Vries *et al.*, Nucl. Instr. Meth. **A223** (1984) 1
- [13] P.C. Dunn, Nucl. Instr. Meth. **224** (1984) 106
- [14] C. Fernandez *et al.*, Nucl. Instr. Meth. **225** (1984) 313
- [15] P. Carlson, Nucl. Instr. Meth. **A248** (1986) 110
- [16] G.S. Kyle *et al.*, Phys. Rev. Lett. **52** (1984) 974
- [17] N. Voegler and J. Friedrich, Nucl. Instr. Meth. **198** (1982) 293
- [18] F. Garibaldi *et al.*, Nucl. Instr. Meth. **A314** (1992) 1
- [19] M. Leuschner *et al.*, Phys. Rev. **C49** (1994) 955
- [20] B. van den Brink Ph. D. Thesis, Vrije Universiteit, Amsterdam (1995)
- [21] I. Bobeldijk *et al.*, Phys. Rev. Lett. **73** (1994) 2684
- [22] M. Benot *et al.*, Nucl. Instr. Meth. **154** (1978) 253
- [23] G. Poelz, Private communication
- [24] G. Poelz, Nucl. Instr. Meth. **A248** (1986) 118
- [25] S.K. Sahu *et al.*, Nucl. Instr. Meth. **A382** (1996) 441
- [26] D. W. Higinbotham, accepted for publication in Nucl. Instr. Meth. (1997)
- [27] M.A. van Uden, Ph. D. Thesis, Universiteit Utrecht (1997); and to be published.
- [28] M. Schroevers, Undergraduate Thesis, Universiteit Utrecht (1997).